Research Article

Shen Zhang, Yue Liang, Xiangqun Qian, David Hui, and Kuichuan Sheng*

Pyrolysis kinetics and mechanical properties of poly(lactic acid)/bamboo particle biocomposites: Effect of particle size distribution

https://doi.org/10.1515/ntrev-2020-0037
received December 12, 2019; accepted December 17, 2019

Abstract: Bamboo particle (BP)-reinforced poly(lactic acid) (PLA) biocomposites were fabricated. The effect of the BP particle size distribution on the pyrolysis and mechanical properties of PLA biocomposites was evaluated. The optimum particle size of BP for improving the tensile strength PLA biocomposites is 200 mesh (16.6–84.5 μm). The pyrolysis mechanism and kinetics were studied according to the Coats–Redfern method. The addition of BP inhibited the pyrolysis process of PLA. The activation energy of biocomposites ranged from 120.7 to 151.5 kJ/mol, which is significantly higher than that of the neat PLA. The pyrolysis mechanisms of biocomposites are attributed to the chemical reaction at low pyrolysis temperature (270–400°C) and ash layer diffusion control at high pyrolysis temperature (400–600°C). Crystallization behavior of biocomposites showed that small BPs in PLA biocomposites generated more cross-linking points in the PLA matrix, which constrained the movement of the molecular chain and acted as an effective nucleating agent in promoting the crystallization process. The pyrolysis behavior and mechanical properties analysis provide critical information for potential large-scale production of the PLA biocomposites.

Keywords: particle size distribution, poly(lactic acid) biocomposites, thermal kinetics

1 Introduction

Traditional polymer products obtained from petroleum have been utilized for several decades and caused nonnegligible environmental issues. Complete degradation of the traditional plastic wastes without contaminating soil, water and air is still difficult to achieve with the current technologies [1]. Degradable biopolymers including poly(butylene succinate), poly(hydroxyalkanoates) and poly(lactic acid) (PLA) derived from renewable natural biomass resources such as starch, straw and chitin have become excellent substitutes for traditional petroleum-based polymer in recent years. PLA is one of the potential biodegradable and bio-based polymer representatives, which have been commercialized in the market for medical, food packaging and pharmaceutical uses [2]. As an aliphatic polyester, PLA has some disadvantages such as poor impact resistance, being flammable and low melting point, which severely limit its application in the fields of electronics, building materials, furniture and logistics packaging [3,4].

To expand the scope of application and reduce the production cost, PLA–natural fiber biocomposites are attracting more research interests for their unique thermal and mechanical properties and low cost [5,6]. However, the key problem during fabrication of PLA/BP biocomposites is the poor interfacial interaction between BP reinforcement and PLA matrix. Interface separation might happen between BP and PLA due to the low compatibility. Alkaline treatment of natural fiber has been proved to be an effect method to modify the surface morphology of fiber and improve mechanical interlocking compatibility. Alkaline treatment removes lignin, hemicellulose, wax and oils, resulting in increasing interfacial bonding strength between lignocellulosic fibers and polymer [7,8]. The natural crystalline structure of the bamboo cellulose is converted to form more stable crystalline structure including Na–cellulose and cellulose-II after alkaline treatment [9]. Moso bamboo, an abundant natural cellulosic resource, has gained much attention in the comprehensive utilization of biomass over the past years due to its abundance, fast growth, regeneration and high productivity [10,11]. Bamboo particle (BP) is one of the biggest industrial processing wastes, especially in China. Large amounts of industrial processing of BPs cause water and soil pollution if it cannot be utilized in the right way. Incineration is a traditional way to dispose these BPs.

* **Corresponding author: Kuichuan Sheng,** College of Biosystems Engineering and Food Science, Zhejiang University, Hangzhou, 310058, China, e-mail: kcsheng@zju.edu.cn
Shen Zhang, Yue Liang, Xiangqun Qian: College of Biosystems Engineering and Food Science, Zhejiang University, Hangzhou, 310058, China
David Hui: Department of Mechanical Engineering, University of New Orleans, New Orleans, LA 70148, United States of America

However, it would discharge sulfur dioxide, nitrogen oxides and dust. Large-scale production of bamboo–PLA biocomposites in green process has paved the way to switch the bamboo waste to renewable resources. Natural fiber–reinforced biocomposites can be degraded or composted without harming environment. Utilization of industrial saw bamboo dust for degradable biocomposites has attracted much attention. The biological functions of BP are carbon dioxide sequestration and biodegradation. Conversely, the advantages of BPs are low cost, low density and acceptable specific strength properties. The key problem during fabrication of PLA/BP biocomposites is the poor interfacial interaction between BP reinforcement and PLA matrix. Interface separation might happen between BP and PLA due to the low compatibility. However, the BP size has a great influence on the properties of PLA biocomposites. To achieve large-scale production of PLA biocomposites, it is necessary to study the effect of BP size distribution on mechanical and thermal stability properties [12].

Modifications of natural fillers affect the degradability and degradation rate of PLA biocomposites. PLA biocomposites with natural fillers are highly flammable. As the initial combustion stage of PLA biocomposites, pyrolysis has great influence on the thermal stability, ignition and heat diffusion process. Furthermore, the thermal stability and degradation kinetics and the pyrolysis product distribution are important factors for determining the molten process, which should be adapted to minimize thermal decomposition [13]. Pyrolysis behavior and related parameters are crucial for the industrial production process. As the kinetic triplet, activation energy, pre-exponential factor and the reaction model can be used to illustrate the thermal degradation kinetics [14]. The polymer behavior in different thermal conditions can be deduced based on kinetics, which will be useful for later specific applications. Pal et al. investigated the thermal kinetics of nanoamphiphilic chitosan dispersed PLA biocomposites films by TG-FTIR analysis. Results showed that the thermal stability of PLA biocomposites decreased with the increase of nanoamphiphilic chitosan. It may attribute to the intermolecular distance and enrichment in chain mobility [15]. However, few studies focus on a detail investigation about pyrolysis degradation of PLA/BP biocomposites and the effects of BP size distribution on the mechanical of PLA biocomposites.

Herein, we prepared alkali-treated BP-reinforced PLA biocomposites. The effects of particle size distribution (PSD) and different concentrations of NaOH solvent on the mechanical and pyrolysis properties of PLA/BP biocomposites were investigated. The toughening effect of BPs with different PSD-reinforced PLA biocomposites was investigated based on the three-level failure analysis model [16]. The pyrolysis mechanism and the kinetics model of biocomposites were analyzed by the thermogravimetric analysis (TGA) and the Coats–Redfern method. This study provided an essential reference for the preparation of PLA–lignocellulose biocomposites.

2 Experimental

2.1 Materials

BPs were supplied by a local moso bamboo processing factory, Lin'an, Zhejiang Province, China. PLA (4032D) was purchased from Tongjieliang Bio-Materials Co., Ltd, Shanghai, China. The molecular weight of PLA (4032D) is 16,000 g/mol. All other reagents and solvents were used as received from the commercial source without further purification.

2.2 Fabrication of PLA/BP biocomposites

PLA pellets were dried (55°C) over night. BP was immersed in 0.3 mol/L NaOH with the solid-to-liquid ratio of 1:15 at 40°C for 3 h and washed with DI water until the BP was alkaline free [17]. Then, BP was dried in the oven at 105°C overnight, and modified BP and PLA matrix were mixed at the ratio of 3:7 according to our previous study [18]. The blends were mixed and melted in a compounding machine with double roll (HL-200, Science and Education Instrument Factory of Jilin University, China) under the conditions of 180°C and 50 rpm. The blends after compounding were fed into an injection molding machine (WZS10D) for extrusion injection to form a biocomposites sample at 195°C and 5 MPa and maintained for 10 s.

BPs were sieved into different particle sizes by 60, 100, 200 and 300 mesh screens and named as BP-*Y*. *Y* represents the mesh of screen. PSD of BP was analyzed by particle size analyzer. Then, the alkali pretreatment of BPs and fabrication of PLA/BP biocomposites were conducted. PLA biocomposites were named PLA/BP. All samples were kept in a desiccator for further characterization.

2.3 Characterization

2.3.1 PSD

Approximately 1.0 g of BP was exposed to a particle size tester (Malvin MS 3000) for the PSD analysis.

2.3.2 Mechanical

Tensile and flexural tests of samples were performed on a universal testing machine at room temperature (CMT4503, MTS Inc.) according to ASTM D638 and ASTM D790. The gauge length and the crosshead speed for the tensile test were set at 50 and 20 mm/min, respectively. The thickness and total length of the specimen for tensile were 4 and 150 mm, respectively. Three specimens were tested [18,19].

2.3.3 Morphological analysis

The fractural surface of the PLA/BP-*Y* biocomposites was scanned by SEM using an SU8010 microscope (Hitachi, Japan) with an accelerating voltage of 4.0 kV. Samples were sprayed with gold film before imaging.

2.3.4 Differential scanning calorimetry (DSC) analysis

DSC (200F3, Netzsch) was adopted to study the thermal properties of pure PLA and PLA/BP biocomposites. About 10.0 mg of dry biocomposites or PLA was weighed and hermetically sealed in an aluminum crucible. Samples were heated from 0 to 180°C at a rate of 10°C/min with N_2 flow at 50 mL/min and held isothermally for 3 min, followed by cooling down to 0°C and reheated up to 180°C at a rate of 10°C/min. An empty aluminum crucible was used as the reference. The second heating process was recorded for further evaluation. Cold crystallinity (X_{cc}) was estimated according to the following equation (1).

$$X_{cc} = \frac{\Delta H_m - \Delta H_{cc}}{\Delta H_0 \times X_{PLA}} \tag{1}$$

where ΔH_{cc} refers to the crystallization enthalpy of biocomposites and ΔH_0 refers to the enthalpy value during 100% crystallization of PLA, which is 93.6 J/g [20]. X_{PLA} refers to the weight ratio of PLA in PLA/BP biocomposites.

2.3.5 TGA

TGA was conducted in nitrogen atmosphere at a flow rate 50 mL/min with a heating rate of 20°C/min from room temperature to 600°C to measure the pyrolysis characteristics of the biocomposites (TGA-60A, Shimadzu, Japan). All pyrolysis parameters were calculated using TA-60 [21].

2.4 Kinetic modeling

The kinetic equation for the thermal reactions of PLA and biocomposites is expressed based on the decomposition rate of samples described as follows:

$$\frac{d\alpha}{dt} = kf(\alpha) \tag{2}$$

where α is the conversion fraction obtained from the TG-DTG data, $\frac{d\alpha}{dt}$ refers to the rate of conversion at time t, and α can be expressed as equation (2).

$$\alpha = \frac{m_0 - m_t}{m_0 - m_f} \tag{3}$$

where m_0 is the initial mass of the sample, m_t is the mass of the sample at time t, and m_f is the final mass of the sample. k is the reaction rate constant given by the Arrhenius equation:

$$k = A\exp\left(-\frac{E_a}{RT}\right) \tag{4}$$

where E_a (J/mol) is the activation energy of the reaction, A is the preexponential factor, and T is the thermodynamic temperature.

Combining both expressions, the experimental rate of reaction can be formulated as follows:

$$\frac{d\alpha}{dt} = A\exp\left(-\frac{E_a}{RT}\right)(1-\alpha)^n \tag{5}$$

For a heating rate β (K/min), $\beta = \frac{dT}{dt} = \frac{dT}{d\alpha} \times \frac{d\alpha}{dt}$, equation (4) can be transformed into:

$$\frac{d\alpha}{dT} = \frac{A}{\beta}\exp\left(-\frac{E_a}{RT}\right)(1-\alpha)^n \tag{6}$$

Therefore,

$$\frac{d\alpha}{(1-\alpha)^n} = \frac{A}{\beta}\exp\left(-\frac{E_a}{RT}\right)dT \tag{7}$$

Integrating equation (7) becomes:

$$F(\alpha) = \int_0^x \frac{d\alpha}{(1-\alpha)^n} = \int_{T_0}^{T} \frac{A}{\beta}\exp\left(-\frac{E_a}{RT}\right)dT \tag{8}$$

where $F(\alpha)$ is the integral function of conversion.

In this study, the kinetic parameters of the combustion process were derived by the Coats–Redfern approximation

method [22]. Therefore, equation (8) can be transformed into equation (9) as follows:

$$\ln\left[\frac{F(\alpha)}{T^2}\right] = \ln\left[\frac{AR}{\beta E}\left(1-\frac{2RT}{E}\right)\right] - \frac{E}{RT} \quad (9)$$

For easy calculation, equation (9) can be described as follows:

$$\ln\left[\frac{F(\alpha)}{T^2}\right] = \ln\left(\frac{AR}{\beta E}\right) - \frac{E}{RT} \quad (10)$$

3 Results and discussion

3.1 PSD and morphology of BP

The SEM images of BP before and after the alkali treatment are shown in Figure 1. There are some fine disorderly microfibrils on the surface of BP, resulting in relatively rough surface. The inorganic impurities, lipids and part of hemicellulose on the surface were eliminated. Some pores were formed on the surface, which can produce the strong capillary effect, making the PLA easier to infiltrate the bamboo fiber and enhance the interfacial force between PLA matrix and alkali-treated BP.

Table 1 shows the PSD and specific surface area of BP before the alkaline treatment. The particle sizes of BP-200 and BP-300 are less than 100 μm. The specific surface area of BP increased with the decrease of particle size. The roughness of the BP surface is favorable for the formation of good interfacial diffusion and mechanical interlocking at the PLA interface. The size and the specific surface area of BPs have significant influence on the mechanical properties of the biocomposites. Figure 2 shows the PSD of BP. The particle size of BP-60 and BP-100 ranges from 0 to 550 nm. The particle size of BP-200 and BP-300 ranges from 0 to 150 nm. Figure 3 shows the relationship of S_{BET} (specific surface area) and the pore size of BP. The curve represents the roughness of BP's surface. The pore

Table 1: Particle size analysis of BPs

Sample	D_v (10%) (μm)	D_v (50%) (μm)	D_v (90%) (μm)	Specific surface area (m^2/g)	Total volume (m^3/g)
BP-60	56.5	163.0	383.0	63.8	0.0363
BP-100	27.9	120.0	353.0	101.9	0.0233
BP-200	16.6	43.3	84.5	248.4	0.0324
BP-300	7.4	28.7	75.8	561.5	0.0225

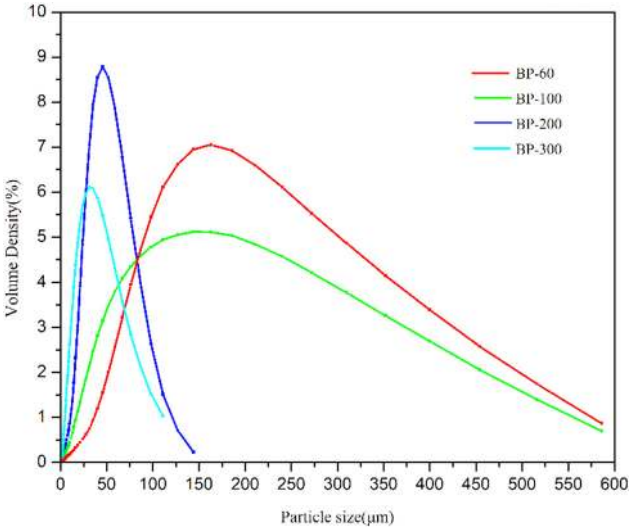

Figure 2: Particle size distribution of BP.

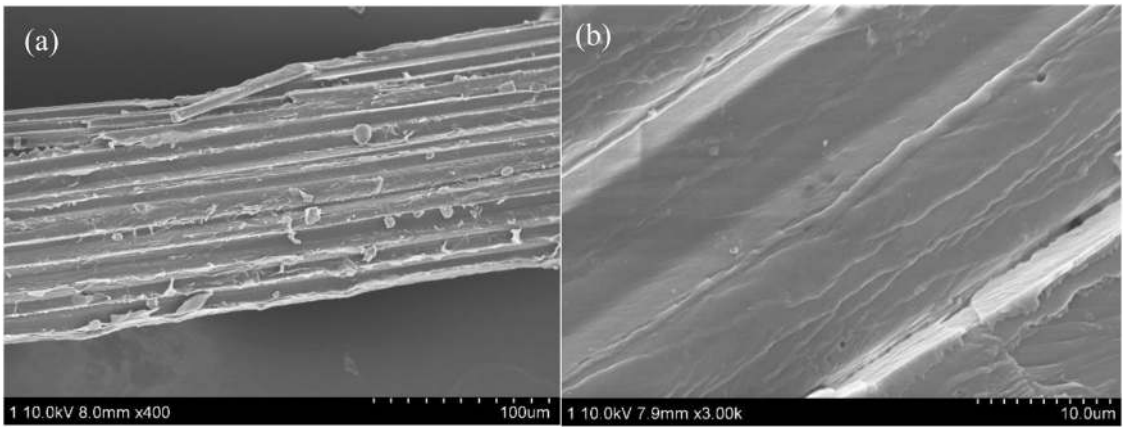

Figure 1: SEM images: (a) untreated BP, (b) BP after alkali treatment.

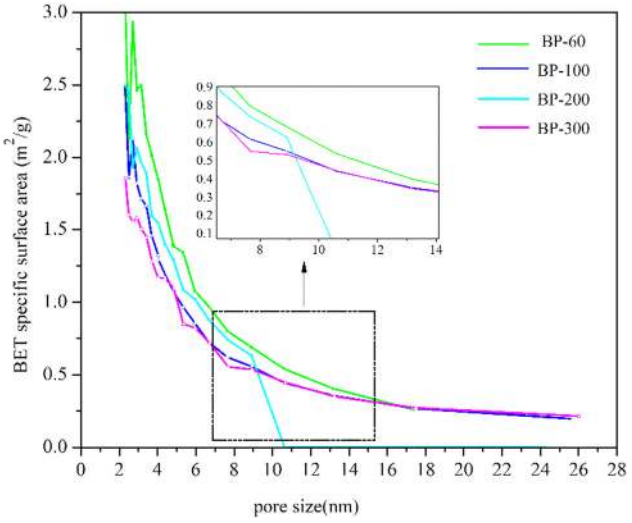

Figure 3: Pore size and S_{BET} of BP.

size of BP ranges from 2 to 26 nm. The roughness of BP increases with the increase of particle size of BP. It may attribute that the bigger paticle size have more pore on the surface of particle. BP-200 have bigger S_{BET} than that of BP-100. However, the pore size of BP-200 ranges from 2 to 10 nm, which is samller than that of BP-100.

3.2 Mechanical properties

Figures 4 and 5 show the tensile and flexural properties of PLA biocomposites, respectively. With the increase of particle size, Young's modulus decreased. It indicates that the resistance ability to deformation decreased with the decrease of particle size. The flexural strength and modulus of biocomposites reached the maximum of 48.1 and 5503.3 MPa with the addition of BP-200, respectively,

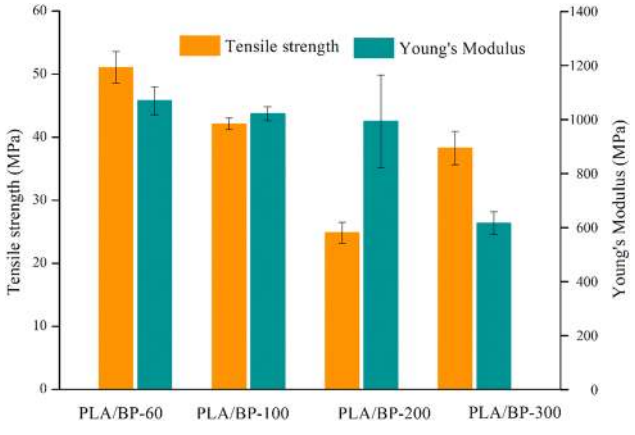

Figure 4: Tensile properties of PLA/BP biocomposites reinforced by BP with different PSD.

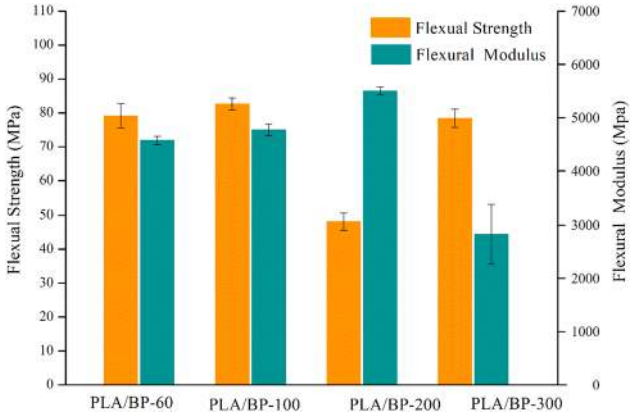

Figure 5: Flexural properties of PLA/BP biocomposites reinforced by BP with different PSD.

and then decreased with the addition of BP-300. Compared with other biocomposites, flexural modulus and flexural strength of PLA/BP-300 decreased significantly. It can be seen from Figure 5 that the flexural strength of PLA/BP-*X* improved significantly, compared with that of PLA/BP. It may be caused by the hydrogen bonding formed between the hydroxyl on the BP and PLA molecules, which improved the interfacial interaction.

The three failure mode levels, namely, a bond break mode at the atomistic level, fiber failure mode at the mesoscopic level and macroscopic crack propagation at the macroscopic level, were used to analyze the mechanical properties of biocomposites. BPs with different PSDs were modified under the same alkaline treatment condition. So, the bond break at the atomistic level is in the same situation [23]. Fiber failure mode at the mesoscopic level and macroscopic crack propagation at the macroscopic level were the main reasons to explain the performance of biocomposites in tensile and flexural experiments. Mesoscale fiber breakage and interfacial debonding were the main destruction modes in PLA/BP-60, PLA/BP-100 and PLA/BP-200 in the flexural experiment [24]. The particle size of BP-300 ranges from 7.4 to 75.8 μm, resulting in the interfacial debonding in the flexural experiment.

3.3 DSC

DSC curves of PLA/BP are shown in Figure 6. Table 2 lists the thermal property parameters of the PLA/BP biocomposites, including the crystallization temperature T_c (°C), glass transition temperature T_g (°C), crystallization enthalpy ΔH_c (J/g), crystallinity X_c (%), melting temperature T_m (°C) and melting enthalpy ΔH_m (J/g).[25].

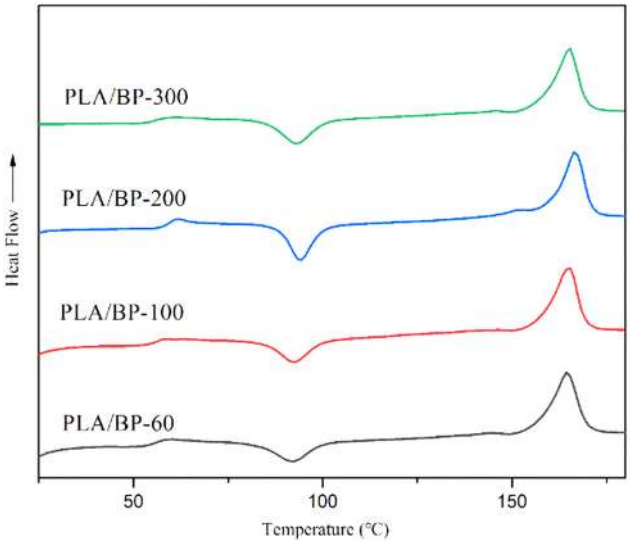

Figure 6: The DSC thermograms of PLA and PLA/BP biocomposites.

The addition of BP decreased the T_g and T_{cc} of the PLA matrix. This is because the introduction of BP destroys the chemical structure of the PLA molecule, reduces the interaction between the PLA molecular chains and enhances the mobility of the molecular segments [26]. Compared with T_g of PLA/BP biocomposites, T_c of PLA/BP-*X* increased slightly, indicating that the NaOH solution treatment improved the interfacial compatibility of the composite. The PLA/BP-0.3 has the highest T_g and T_c of 56.3 and 92.0°C, respectively. It is indicated that the nucleation effect of BP-0.3 and the PLA matrix improved.

As shown in Table 2, no obvious relationship among glass transition temperature, cold crystallization temperature and BP size was observed. The interaction between PLA polymer chains is weakened, and the flexibility of the molecular chain increased, which is more conducive to the movement of the molecular segments [27].

The BPs act as an effective nucleating agent in promoting the crystallization process compared with neat PLA. The crystallinity of the biocomposites was increased, which could affect the strength and modulus of the

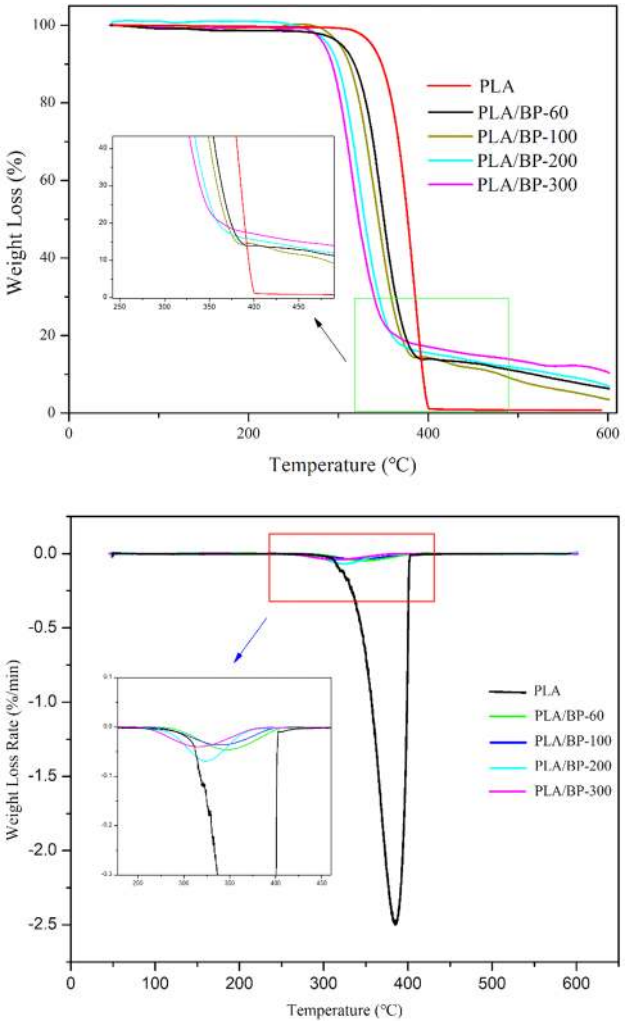

Figure 7: TG and DTG curves of biocomposites.

biocomposites. PLA/BP-300 has higher crystallinity than PLA/BP-200. It may be explained by the fact that the BP with smaller particle size dispersed more uniformly in the PLA matrix and generated more cross-linking points in the PLA matrix than that of large ones, which constrained the movement of the molecular chain [36]. The addition of BP with different PSD had a significant effect on the crystallization behavior and melting behavior of PLA.

Table 2: Thermal characteristics parameters of PLA/BP biocomposites

Samples	T_g (°C)	T_c (°C)	ΔH_c (J/g)	X_c (%)	T_m (c)	ΔH_m (J/g)
PLA	40.8	97.8	15.4	36.6	157.1	34.28
PLA/BP-60	56.3	92.0	14.9	26.4	164.5	32.2
PLA/BP-100	56.5	92.4	14.5	24.5	165.0	23.9
PLA/BP-200	54.5	88.8	17.5	13.3	161.3	26.3
PLA/BP-300	56.1	93.1	16.1	22.4	165.2	30.8

3.4 TGA

As shown in Figure 7, the addition of BP decreased the pyrolysis rate of PLA significantly. The DTG curve is the first derivative of the TG curve. This is because the pyrolytic biochar obtained from the pyrolysis process prevents heat from spreading. The temperature intervals and weight loss at each distinct zone were summarized in Table 3. The whole pyrolysis process of PLA and biocomposites depicted three distinct zones according to the TG curves. Zone 1, 2 and 3 of neat PLA represented the water evaporation phase, devolatilization, pyrolysis phase and char pyrolysis phase, respectively [28]. The scission of hydrogen bonds including intrachain and interchain hydrogen in cellulose happened in zone 1, producing oligomers of glucose. There was a quick weight loss of PLA in zone 2 at the temperature ranged from 311 to 405°C. With the increase of temperature, the weight of PLA almost maintained invariable in zone 3. PLA and BP have a synergistic effect in the pyrolysis process in zone 2, where free radicals generated by BP pyrolysis promoted PLA polymer chain scission and participated in radical transfer reaction. The temperature intervals of the biocomposites in zone 1 were 45–275°C. The first section of pyrolysis is mainly pyrolysis gasification of water and small molecular substances in the BP. The biocomposites went through a quick weight loss in zone 2 (Table 4). The weight loss of biocomposites in zone 2 was less than that of PLA. This may be because the pyrolysis process is an exothermic reaction that accelerates the degradation of the biocomposites. An obvious decrease of weight loss and narrowed temperature intervals in zone 2 were observed with the decrease of particle size. It indicates that the BPs with smaller particle size are in favor of preventing the pyrolysis process and improving the thermal stability of the biocomposites. As shown in zone 3, the residual weight of the biocomposites are significantly higher than that of PLA, which may be attributed to the fact that the alkali introduced during pretreatment was converted to irrecoverable salts or incorporated as salts, which provides higher thermal stability to the BP during the alkali pretreatment [29].

3.5 Kinetic analysis

The pyrolysis kinetic parameters are important for understanding the pyrolysis of PLA/BP biocomposites, which are relevant for potential applications and thermal recycling [30,31]. The apparent activation energy values of the biocomposites pyrolysis obtained by the Coats–Redfern method were summarized in Table 3. The activation energies (E) and the pre-exponential factor (A) are key kinetic parameters to explore the pyrolysis mechanism of the biocomposites and PLA [32]. The preexponential factor indicates the reaction rate at which the molecule participates in the chemical reaction. A larger pre-exponential factor indicates the faster reaction rate of the sample at the same temperature [33]. The

Table 3: Weight loss at different temperature intervals during combustion of samples

Sample	Zone 1		Zone 2		Zone 3	
	Temperature intervals (°C)	Weight loss (%)	Temperature intervals (°C)	Weight loss (%)	Temperature intervals (°C)	Weight loss (%)
PLA	45–309	0.05	309–405	97.98	405–600	1.07
PLA/BP-60	45–274	1.97	274–368	75.37	368–600	16.64
PLA/BP-100	45–288	1.93	288–363	76.55	363–600	18.04
PLA/BP-200	45–274	2.00	274–344	69.47	344–600	21.58
PLA/BP-300	45–273	2.00	273–335	66.51	335–600	21.09

Table 4: Pyrolysis kinetic parameters of BP, PLA and biocomposites

Sample	Zone 2				Zone 3			
	E (kJ/mol)	A (min^{-1})	R^2	Mechanism	E (kJ/mol)	A (10^{-3} min^{-1})	R^2	Mechanism
PLA	70.3	0.9×10^{11}	0.981	A1	–	–	–	–
PLA/BP-60	120.7	0.8×10^{11}	0.963	A1	49.1	0.103	0.987	D1
PLA/BP-100	144.6	1.1×10^{13}	0.957	A1	44.1	0.104	0.988	D1
PLA/BP-200	135.6	3.9×10^{12}	0.962	A1	45.3	0.105	0.963	D1
PLA/BP-300	151.5	1.9×10^{14}	0.961	A1	45.5	0.107	0.945	D1

Table 5: The kinetic models used in solid state reactions

Reaction model	$F(\alpha)$	Code
Chemical reaction		
First order	$-\ln(1-\alpha)$	A1
*n*th order	$(n-1)^{-1}-(1-\alpha)^{(1-n)}$	A*n*
Diffusional		
1-D	α^2	D1
2-D	$(1-\alpha)\ln(1-\alpha)+\alpha$	D2
3-D (Jander)	$[1-(1-\alpha)^{1/3}]^2$	D3
3-D (Ginstling–Brounshtein)	$1-\frac{2\alpha}{3}-(1-\alpha)^{2/3}$	D4

weight loss of PLA and biocomposites in zone 1 is due to moisture loss [34]. Based on the fitting results of linear regression by the expressions of $F(\alpha)$ in Table 5, zone 2 was fitted by model A1 with high correlation coefficients (R^2) from 0.957 to 0.981. The activation energy of biocomposites ranged from 120.7 to 151.5 kJ/mol, which was significantly higher than that of PLA (70.3 kJ/mol) in zone 2. It can be concluded that the addition of BP increases the activation energy of the process. The mechanism of pyrolysis of PLA and biocomposites in zone 2 is chemical reaction. The PLA and alkali-treated BP were decomposed in zone 2. It may be attributed to the combined pyrolysis process of alkali-treated BP and PLA. With the decrease of particle size, the pre-exponential factor of biocomposites decreased in zone 2 and increased in zone 3. The alkali- treated BP act as a thermal barrier in the PLA matrix. The BP particle with a larger size has a better effect in preventing the pyrolysis of the biocomposites in zone 2. The bamboo charcoal with high content of ash was formed in high temperature zone 2 [35], resulting in diffusion resistance in zone 3. Zone 3 was fitted by model 1-D, and the mechanism of pyrolysis process is ash layer diffusion control. According to the results, the kinetic of the biocomposites pyrolysis could be applied to adjust the processing parameters of the biocomposites, such as the addition of flame retardant and the process of extrusion and injection molding.

3.6 Morphology

The SEM images of fracture of the biocomposites are shown in Figure 8. The particle size of BP had significant effects on the interface between PLA and BP. The broken BP was

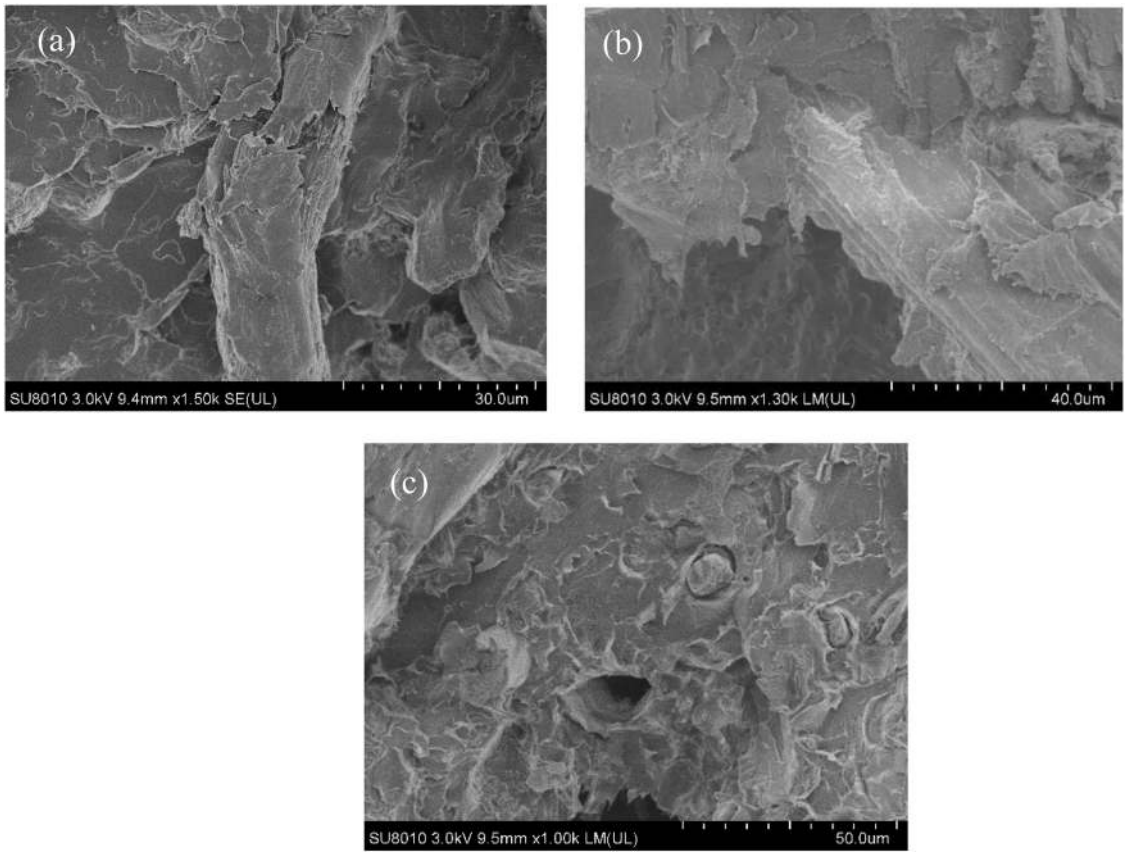

Figure 8: SEM micrographs of fracture surface of biocomposites: (a) PLA/BP-60, (b) PLA/BP-100 and (c) PLA/BP-200.

observed in Figure 8(a) and (b). The PLA matrix underwent elongational deformation along the stretching direction, which improve the interface effect between BP and PLA. With the decrease of the particle size, the holes on the fracture surface of biocomposites were observed in Figure 8(c). The BP-200 could not bear the stress in the PLA matrix and the interface bonding strength on the microscopic surface decreased, resulting in the macroscopic mechanical properties including the decreased tensile and flexural properties [37]. It can be proved intuitively from the SEM images that the toughening failure mode of bamboo fiber changes from mesoscale fiber break to interfacial adhesion with the decrease in the particle size.

4 Conclusion

The PSD of BP has great influence on the mechanical properties of the biocomposites. The optimum particle size of BP for improving the tensile strength PLA biocomposites is 200 mesh. The addition of BP decreased the pyrolysis rate and improved the activation energy of the biocomposites compared with the neat PLA. The main decomposition stage of biocomposites was in zone 2, while the PLA was decomposed in zone 2. Interaction between the PLA and BPs inhibited the pyrolysis process. The activation energies of the biocomposites in zone 2 and zone 3 range from 44.1 to 151.5 kJ/mol, respectively, while for neat PLA were 70.3 kJ/mol in the zone 2. The chemical reaction and diffusion occurred in zone 2 and zone 3, respectively. The results of this study provide theoretical support for the potential pilot-scale production of the degradable PLA biocomposites.

Acknowledgments: This work was financially supported by the National Natural Science Foundation of China (31971794) and Key Research & Development Projects of Zhejiang Province (2019C02080).

Conflict of interest: The authors declare no conflict of interest regarding the publication of this paper.

References

[1] Ali A, Phull AR, Zia M. Elemental zinc to zinc nanoparticles: is ZnO NPs crucial for life? Synthesis, toxicological, and environmental concerns. Nanotechnol Rev. 2018;7(5):413–941.

[2] Kamal MR, Khoshkava V. Effect of cellulose nanocrystals (CNC) on rheological and mechanical properties and crystallization behavior of PLA/CNC nanocomposites. Carbohyd Polym. 2015;123:105–14.

[3] Nagarajan V, Zhang K, Misra M, Mohanty AK. Overcoming the fundamental challenges in improving the impact strength and crystallinity of PLA biocomposites: influence of nucleating agent and mold temperature. ACS Appl Mater Interfaces. 2015;7(21):11203–14.

[4] Sharma AK, Sahoo PK, Majumdar DK, Panda AK. Topical ocular delivery of a COX-II inhibitor via biodegradable nanoparticles. Nanotechnol Rev. 2016;5(5):435–44.

[5] Pracella M, Haque MM, Paci M, Alvarez V. Property tuning of poly(lactic acid)/cellulose bio-composites through blending with modified ethylene-vinyl acetate copolymer. Carbohyd Polym. 2016;137:515.

[6] Pornwannachai W, Ebdon JR, Kandola BK. Fire-resistant natural fibre-reinforced composites from flame retarded textiles. Polym Degrad Stabil. 2018;154:115–23.

[7] Li X, Tabil LG, Panigrahi S. Chemical treatments of natural fiber for use in natural fiber-reinforced composites: a review. J Polym Environ. 2007;15:25–33.

[8] Kalia S, Kaith BS, Kaur I. Pretreatments of natural fibers and their application as reinforcing material in polymer composites – a review. Polym Eng Sci. 2010;49:1253–72.

[9] Orue A, Jauregi A, Peña-Rodriguez C, Labidi J, Eceiza A, Arbelaiz A. The effect of surface modifications on sisal fiber properties and sisal/poly(lactic acid) interface adhesion. Composites Part B. 2015;73:132–8.

[10] Faruk O, Bledzki AK, Fink HP, Sain M. Biocomposites reinforced with natural fibers: 2000–10. Prog Polym Sci. 2012;37:1552–6.

[11] George J, Sreekala MS, Thomas S. A review on interface modification and characterization of natural fiber reinforced plastic composites. Polym Eng Sci. 2010;41:1471–85.

[12] Song WL, Veca LM, Anderson A, Cao MS, Cao L, Sun YP. Lightweight nanocomposite materials with enhanced thermal transport properties. Nanotechnol Rev. 2012;1:363–76.

[13] Valapa R, Pugazhenthi G, Katiyar V. Thermal degradation kinetics of sucrose palmitate reinforced poly(lactic acid) biocomposites. Int J Biol Macromol. 2014;65:275–83.

[14] Ossai CI, Raghavan N. Nanostructure and nanomaterial characterization, growth mechanisms, and applications. Nanotechnol Rev. 2018;7:209–17.

[15] Jandas PJ, Prabakaran K, Mohanty S, Nayak SK. Evaluation of biodegradability of disposable product prepared from poly (lactic acid) under accelerated conditions. Polym Degrad Stabil. 2019;164:46–54.

[16] Chen Y, Wang S, Liu B, Zhang J. Effects of geometrical and mechanical properties of fiber and matrix on composite fracture toughness. Compos Struct. 2015;122:496–506.

[17] Qian S, Mao H, Sheng K, Lu J, Luo Y, Hou C. Effect of low-concentration alkali solution pretreatment on the properties of bamboo particles reinforced poly(lactic acid) composites. J Appl Polym Sci. 2013;130:1667–74.

[18] Wang S, Dai G, Yang H, Luo Z. Lignocellulosic biomass pyrolysis mechanism: a state-of-the-art review. Prog Energ Combust Sci. 2017;62:33–86.

[19] Zhang S, Yao W, Zhang H, Sheng K. Polypropylene biocomposites reinforced with bamboo particles and ultrafine bamboo-char: the effect of blending ratio. Polym Compos. 2018;39:640–6.

[20] Huang Y, Pan P, Shan G, Bao Y. Polylactide-*b*-poly(ethylene-*co*-butylene)-*b*-polylactide thermoplastic elastomers: role of polylactide crystallization and stereocomplexation on microphase separation, mechanical and shape memory properties. RSC Adv. 2014;4:47965–76.
[21] Azizi K, Keshavarz MM, Abedini NH. Simultaneous pyrolysis of microalgae *C. vulgaris*, wood and polymer: the effect of third component addition. Bioresour Technol. 2017;247:66.
[22] Coats A, Wredfern JP. Kinetic parameters from thermogravimetric data. Nature. 1964;201:68–9.
[23] Anwar A, Kanwal Q, Akbar S, Munawar A, Durrani A, Farooq MH. Synthesis and characterization of pure and nanosized hydroxyapatite bioceramics. Nanotechnol Rev. 2017;6:149–57.
[24] Chen YL, Liu B, He XQ, Huang YH, Wang KC. Failure analysis and the optimal toughness design of carbon nanotube-reinforced composites. Compos Sci Technol. 2010;70:1360–7.
[25] Ho MC, Ong VZ, Wu TY. Potential use of alkaline hydrogen peroxide in lignocellulosic biomass pretreatment and valorization – a review. Renew Sust Energ Rev. 2019;112:75–86.
[26] Wang F, Zhou S, Yang M, Chen Z, Ran S. Thermo-mechanical performance of polylactide composites reinforced with alkali-treated bamboo fibers. Polymers (Basel). 2018;10:401.
[27] Zubir NM, Sam ST, Zulkepli NN, Omar MF. The effect of rice straw particulate loading and polyethylene glycol as plasticizer on the properties of polylactic acid/polyhydroxybutyrate-valerate blends. Polym Bull. 2018;75:61–76.
[28] Peng C, Zhai Y, Yun Z, Xu B, Wang T, Li C, et al. Production of char from sewage sludge employing hydrothermal carbonization: Char properties, combustion behavior and thermal characteristics. Fuel. 2016;176:110–8.
[29] Sheng K, Zhang S, Qian S, Fontanillo Lopez CA. High-toughness PLA/Bamboo cellulose nanowhiskers bionanocomposite strengthened with silylated ultrafine bamboo-char. Composites Part B. 2019;165:174–82.
[30] Arrieta MP, Parres F, López J, Jiménez A. Development of a novel pyrolysis-gas chromatography/mass spectrometry method for the analysis of poly(lactic acid) thermal degradation products. J Anal Appl Pyrol. 2013;101:150–5.
[31] Inoue M, Tada Y, Suganuma K, Ishiguro H. Thermal stability of poly(vinylidene fluoride) films pre-annealed at various temperatures. Polym Degrad Stabil. 2007;92:1833–40.
[32] Cai J, Li B, Chen C, Jing W, Min Z, Ke Z. Hydrothermal carbonization of tobacco stalk for fuel application. Bioresour Technol. 2016;220:305–11.
[33] He C, Giannis A, Wang JY. Conversion of sewage sludge to clean solid fuel using hydrothermal carbonization: hydrochar fuel characteristics and combustion behavior. Appl Energ. 2013;111:257–66.
[34] Pandey JK, Chu WS, Kim CS, Lee CS, Ahn SH. Bio-nano reinforcement of environmentally degradable polymer matrix by cellulose whiskers from grass. Composites Part B. 2009;40:676–80.
[35] Kovacevic Z, Bischof S, Fan M. The influence of spartium junceum fibres modified with montmorrilonite nanoclay on the thermal properties of PLA biocomposites. Composites Part B. 2015;78:122–30.
[36] Bisheh H, Wu N, Hui D. Polarization effects on wave propagation characteristics of piezoelectric coupled laminated fiber-reinforced composite cylindrical shells. Int J Mech Sci. 2019;161–2.
[37] Ho MP, Wang H, Lee JH, Ho CK, Lau KT, Leng JS, et al. Critical factors on manufacturing processes of natural fibre composites. Composites Part B. 2012;43:3549–3562.